SABRINA: A SAR Bistatic Receiver for Interferometric Applications

Jesus Sanz-Marcos, Paco Lopez-Dekker, *Member, IEEE*, Jordi J. Mallorqui, *Member, IEEE*, Albert Aguasca, *Member, IEEE*, and Pau Prats, *Member, IEEE*

Abstract—This letter discusses the implementation of SABRINA, Synthetic Aperture radar Bistatic Receiver for Interferometric Applications. The ground resolution of a fixed-receiver bistatic system is studied, showing that it is comparable to that of a monostatic system. Due to the short distance from target to receiver, large sensitivity is obtained. The noncooperative nature of the bistatic system forces a conservative data-acquisition strategy based on continuously sampling the scattered signal during a temporal window around the predicted satellite overpass time. Also, to be able to synchronize the system in time and in frequency, sampling of a direct signal obtained through an antenna pointed at the satellite is required. Besides the signal processing required to phase-lock the received signal, the bistatic synthetic aperture radar processing needs to take into account the azimuth-dependent phase history. First focused images obtained with the SABRINA–ENVISAT combination are discussed.

Index Terms—Bistatic synthetic aperture radar, interferometry, sensor of opportunity, synthetic aperture radar (SAR).

I. INTRODUCTION

A S SYNTHETIC aperture radar (SAR) and associated research areas such as InSAR or Pol-SAR are developing into maturity, bistatic systems are emerging as a new research field. Bistatic systems open the possibility to explore alternative geometries and different scattering mechanisms. Some of the upcoming systems, such as the future Tandem-X mission, can be described as quasi-monostatic, with the receiver and the transmitter close to each other in almost parallel orbits [1]. While these systems present important technological challenges, there are few new theoretical aspects involved. In contrast, if the receiver and the transmitter follow independent trajectories or are located far apart completely, new scenarios arise [2]. Besides the geometry-related issues in the design of bistatic systems, there are a number of synchronization-related challenges. For example, the need for independent reference oscillators on transmit and receive dramatically increases the impact of oscillator phase noise [3]. Synchronization issues are furtherly increased in the case of the noncooperative bistatic

system, in which case, even the pulse-repetition-frequency (PRF) signal needs to be recovered.

Last year, the Remote Sensing Laboratory of the Universitat Politècnica de Catalunya (UPC) has developed a C-band receiver for a ground-based bistatic-SAR system using the European Space Agency's (ESA) ERS-2 and ENVISAT as transmitters of opportunity that has been named SAR bistatic receiver for interferometric applications (SABRINA) [4], [5]. The system is intended to provide an experimental platform with which to study most aspects of the bistatic-SAR systems, including scattering phenomena, processing, and hardware-related aspects with a particular emphasis on those linked to synchronization. This letter presents a system-level discussion of SABRINA.

Section II of this letter begins by addressing the implications of the bistatic geometry considered, discussing the resulting resolution, and presenting the corresponding radar range equation. Section III discusses SABRINA at system level, considering the requirements and constraints, and describing its implementation. In Section IV, some experimental results are presented, and the first focused bistatic-SAR image produced by the system is shown. Finally, we present some conclusions and suggest future lines of work.

II. SYSTEM GEOMETRY

A. Ground Range Resolution

The ground range resolution can be studied by considering the intersection of the isorange surfaces with the ground surface. In the bistatic geometry, these are ellipsoids that, when the narrow transmit beampattern is considered, reduce to 2-D ellipses with foci at the positions of the transmitter and the receiver. Considering a locally flat surface, the ground resolution can be approximated by

$$\Delta r_{\mathrm{g}} = \frac{c}{\Delta f_{\mathrm{c}} \cdot (\sin \theta_{\mathrm{t}} + \sin \theta_{\mathrm{r}})} \tag{1}$$

where Δf_{c} is the chirp bandwidth, and θ_{t} and θ_{r} are the transmit and receive incidence angles, respectively, with respect to the normal-to-the-ground surface (see Fig. 1). Obviously, if both incidence angles are the same, (1) becomes the known monostatic ground resolution. To illustrate the implications of (1), two cases can be considered. First, assuming the typical ENVISAT transmit incidence angle $\theta_{\mathrm{t}} = 23°$ and a nearly grazing receive incidence angle $\theta_{\mathrm{r}} \approx 90°$, a resolution of
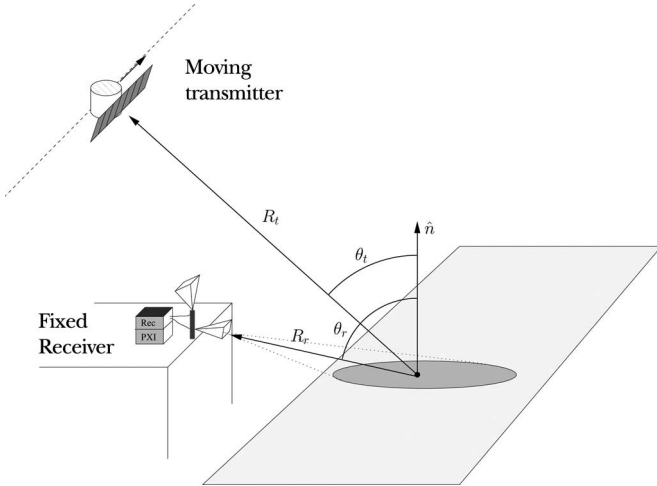
Fig. 1. Bistatic geometry. The figure shows the moving transmitter and the fixed receiver, and the beampattern of the receive antenna covering a portion of the strip illuminated by the transmitter.

roughly 13 m is obtained, much better than the approximately 24-m resolution of the corresponding monostatic case. This case corresponds to what we will loosely refer to as a backscattering geometry. A second case worth considering is a forward-scattering geometry, where the receive antenna is located at the opposite side of the target area with respect to the transmit antenna. In this case we can calculate the resolution assuming a negative incidence angle ($\theta_t = -23°$) which, combined with the nearly grazing conditions on receive, yields a ground resolution of roughly 31 m, which is not far worse than the monostatic resolution.

Studying the denominator of (1), it follows that there is layover if the sum of the incidence and scattered angles

$$\sin \theta_t + \sin \theta_r \qquad (2)$$

changes sign. Also, if the specular scattering condition is met

$$\theta_{t,\text{spec}} = -\theta_{r,\text{spec}} \qquad (3)$$

the sum is zero, resulting in total loss of resolution. It is easy to conclude that this condition is much more likely to occur in a forward-scattering configuration.

B. Azimuth Resolution

The azimuth resolution of a SAR system can be related to the Doppler bandwidth and the velocity of the moving platform. Because of frequency–time duality, a Doppler bandwidth of Δf_d can be inverted to obtain a temporal resolution which, multiplied by the platform velocity v_{sar}, yields the resolution in azimuth:

$$\Delta r_a = \frac{v_{\text{sar}}}{\Delta f_d}. \qquad (4)$$

In the monostatic case, Δf_d is related to the two-way antenna azimuthal beamwidth of the transmit–receive antenna $B_{2\text{-way}}$. For an antenna of length L_a, assuming a two-way beamwidth

equal to λ/L_a yields the usual expression of the azimuth resolution as $L_a/2$.

In the bistatic case, assuming a fixed receiver, the Doppler bandwidth is

$$\Delta f_{d,\text{bist}} = \frac{v_{\text{sar}} B_{1\text{-way}}}{\lambda} \qquad (5)$$

where $B_{1\text{-way}}$ is the one-way transmit beamwidth. Approximating the beampattern by a Gaussian function, the ratio between the one- and two-way beampatterns is $\sqrt{2}$. Hence, the resulting bistatic azimuth resolution is

$$\Delta r_{a,\text{bist}} = \frac{L_a}{\sqrt{2}} = \sqrt{2} \cdot \Delta r_{a,\text{mono}}. \qquad (6)$$

Summarizing, with respect to the monostatic geometry, there are two opposite effects: a factor 2 resolution loss due to the one-way Doppler shifts that are partially compensated by an increased observation time.

C. Radar Range Equation

For a resolution cell with bistatic normalized radar cross section σ^0, the SNR after SAR processing can be obtained following the steps of the derivation for the monostatic case [6]. This results in

$$\text{SNR}_{\text{bist}} = \frac{B_{2\text{-way}}}{B_{1\text{-way}}} \frac{P_{\text{av}} G_t G_r \lambda^3 \sigma^0 \Delta r_g}{(4\pi)^3 R_t R_r^2 k T_0 F_r v_{\text{sar}}} \qquad (7)$$

where G_t and G_r are the transmit and receive gains, respectively, R_t and R_r are the distances from the target to the transmitter and the receiver, T_0 is the system temperature, F_r is the receiver noise figure, and P_{av} is the average radiated power. Note that this expression is only valid for the fixed-receiver scenario. For a given transmit power, the monostatic and bistatic SNRs differ by orders of magnitude, their ratio being proportional to

$$\frac{\text{SNR}_{\text{bist}}}{\text{SNR}_{\text{mono}}} \backsim \frac{G_r R_t^2}{G_t R_r^2}. \qquad (8)$$

III. SYSTEM IMPLEMENTATION

The principal challenge in the implementation of SABRINA has been the synchronization of the receiver with the spaceborne SAR system of opportunity. Since there is no mechanism to explicitly synchronize the receiver with the transmitter, this synchronization needs to be done using the transmit radar signals. Following the same approach used in, for example, GNSS-R [7] systems, the receiver has, in addition to the antenna that illuminates the target area, a second antenna pointed directly at the transmitter in order to obtain a clean replica of the transmit signal.

A. RF Subsystem

In the bistatic geometries considered, the receiver, placed on a building or a tower, is relatively close to the target area.
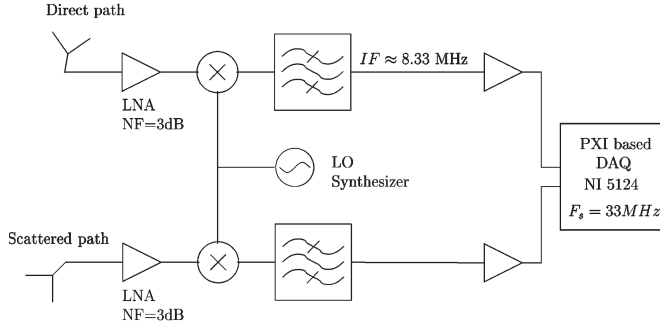
Fig. 2. Receiver diagram of the dual channel receiver. The first channel is connected to an antenna pointed directly at the satellite to obtain a clean reference signal. The second channel receives the scattered signal. Both signals are downconverted to an IF = $f_\mathrm{s}/4$ and are sampled continuously.

Considering (8), this gives an enormous boost in sensitivity (noise equivalent σ^0) with respect to the associated monostatic system. For example, at 1-km distance and using ENVISAT, the $(R_\mathrm{t}/R_\mathrm{r})^2$ factor gives a 58-dB gain. A fraction of this relative gain can be used to relax the sensitivity requirements of the receiver. A large portion, however, is compensated by the lower directivity of the receive antenna, which needs to have a relatively wide beam in order to have a sufficiently large field of view. The current prototype uses an 18-dBi-gain pyramidal horn antenna with a 21° 3-dB beamwidth in azimuth.

The distance from the target to the receiver can range from tens of meters up to several kilometers. This implies that, after processing, the dynamic range can easily exceed 50 dB on top of the dynamic range of σ^0. Allowing for a 30-dB dynamic range for σ^0, an 80 dB of total dynamic range is required, of which, with ENVISAT, roughly 26 dB is provided by the pulse (range) compression. Therefore, the receiver front end requires over 50 dB of dynamic range.

For the direct signal, the SNR at the output of the receiver's front end is given by Friis power transmission equation

$$\mathrm{SNR_d} = \frac{P_\mathrm{t} G_\mathrm{t} G_\mathrm{r} \lambda_0^2}{(4\pi)^2 R_\mathrm{t}^2 k_B \cdot (T_\mathrm{ant} + (F-1)T_\mathrm{sys}) B} \qquad (9)$$

where the antenna temperature T_ant, since it is pointing almost at zenith, is significantly lower than the system's temperature, and B is the signal bandwidth. For ENVISAT, taking the 16-MHz chirp bandwidth and assuming a noise figure of 3 dB and a receive-antenna gain of 18 dB, the expected peak SNR would be in excess of 56 dB.

The dual channel C-band receiver implemented (see Fig. 2) uses a video-band sampling strategy. The received signal, centered roughly at 5.3 GHz, is downconverted to an intermediate frequency equal to $f_\mathrm{s}/4$, a fourth of the sampling rate. In-phase and quadrature demodulation is done digitally in post-processing. The local oscillator is generated using a frequency synthesizer in order to tune the receiver to ENVISAT or ERS-2 center frequency (5.331 and 5.300 GHz, respectively). The RF amplifying stages provide 51 and 35 dB, respectively, for the reflected and direct channel to provide similar voltage levels to the digitizer.

B. Data Acquisition

The data-acquisition subsystem needs to satisfy the following requirements.

1) It should have enough resolution to accommodate the dynamic margin of the reflected signal. It is also desirable that quantization noise does not degrade the SNR of the direct signal. Using the results in the previous section, at least 9 bits of resolution is required.
2) Given the IF sampling solution, each real channel needs to be sampled at least at $2B = 32$ MHz to satisfy Nyquist's criterion.
3) The duration of the acquisition is set by the time during which the imaged region is illuminated by the transmitter. This time, it can be expressed as

$$T_\mathrm{a} = \frac{R_\mathrm{t} B_{1\text{-way}}}{v_\mathrm{sar}} + \frac{R_{\mathrm{r,max}} \Delta\theta_\mathrm{FOV}}{v_\mathrm{sar}}. \qquad (10)$$

The first term in (10) is the illumination time of a single point target, while the second term is determined by the maximum range to the receiver and the angular width of the field of view $\Delta\theta_\mathrm{FOV}$. If the receiver is close to the target region, the second term can be ignored. Under this assumption, for the case of ENVISAT, the observation time is roughly 0.9 s.
4) The acquisition window needs to be synchronized with the satellite overpass.

The short window of opportunity, combined with the long orbit repetition period of the satellites (35 days for ENVISAT and ERS-2 for any particular incidence angle and direction), calls for a conservative acquisition strategy that consists of a continuous sampling during an acquisition window centered at the predicted overpass time. The expected satellite overpass time, the instant when the transmitter is closest to the target area, is calculated using the simplified general perturbations version 4 (SGP4) orbit propagation algorithm [8], which is used as an input two-line Keplerian-element (TLE) sets which can be downloaded from a number of sources (for example, from the space-track portal available at http://space-track.org). The acquisition window needs to be long enough to accommodate prediction errors, which in practice, have been found to be of less than half a second.

SABRINA's acquisition subsystem is implemented using a PXI-based system featuring an off-the-shelve national instrument PXI-5124 card, providing a 12-bit resolution and a sampling rate up to 200 MHz. By continuous sampling at 33 MS/s, the onboard memory provides a continuous-sampling window of 7.6 s.

C. Signal Processing

The biggest challenges in the development of SABRINA relate to the processing of the received signals, which can be broadly divided into two parts:

1) raw data formation;
2) range and azimuth compression.

Raw data formation implies converting the 1-D data stream received to the 2-D range-time data set required by the SAR
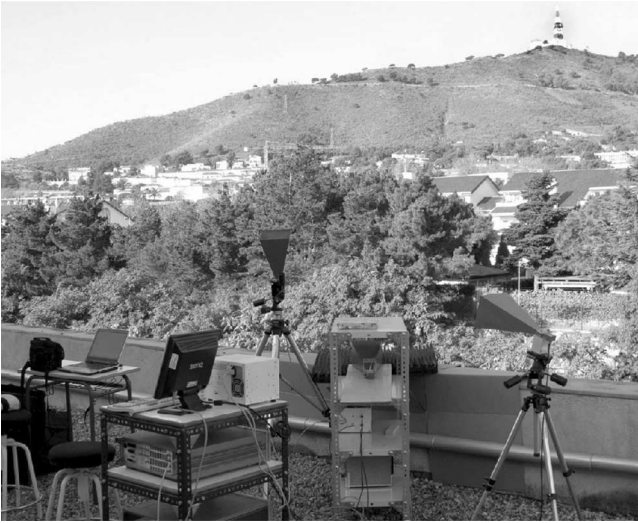
Fig. 3.   SABRINA prototype deployed on the roof of a building at the UPC Campus during an acquisition. One antenna points at the ENVISAT, while the second antenna points west toward the region of interest, which is the Sant Pere Martir Hill (in the background).
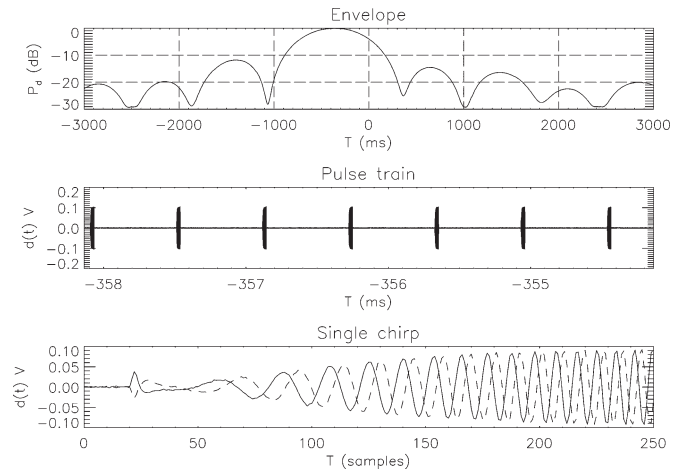

Fig. 4.   Envelope of received signal at the direct channel (top), 5-ms section showing a train of pulses (middle), and detail of two consecutive pulses showing the chirp waveform (bottom).

processing algorithm. This is done implicitly in the monostatic systems or in the cooperative bistatic system (such as the future Tandem-X mission). However, in the noncooperative system, the lack of an explicit synchronization between the transmitter and the receiver poses a set of important challenges: There is no common absolute time frame, there is no explicit PRF signal at the receiver, and the transmitter and the receiver are not phase-locked to each other. This lack of phase synchronization causes an unknown apparent Doppler shift and introduces a phase-noise term that is not present in the monostatic systems. The direct signal is used to recover the PRF signal, after which the data can be organized by pulses. Then, knowledge of the phase history of the direct signal is used to phase-correct the received data.

The extreme bistatic geometry considered results in an azimuth-dependent phase history that, compared to strip mode algorithms, requires new processing strategies. The processing method used in this letter [5], [9] is based on the classical monostatic range-Doppler algorithm for SAR focusing but is extended to the bistatic azimuth invariant topography-dependent case. The main idea is to apply an approximation of the given geometry for a series of subapertures. In the first step, a digital elevation model (DEM) of the illuminated scene is used to calculate a bistatic slant-range map for each transmitted pulse. The second step is to divide the image into subapertures, obtaining for each an azimuth averaged slant-range elevation map. Then, in the range-Doppler domain, classical range cell migration compensation is performed with an added expression to consider the receiver–target distance.

IV. EXPERIMENTAL RESULTS

Throughout its development, SABRINA has been tested locally from the roof of a building at the UPC Campus in Barcelona. Fig. 3 shows the SABRINA prototype setup for a test. The test area is northwest of the campus and includes the Sant Pere Martir Hill, which can be seen in the background

of the picture. During each 35-day orbit repetition period, there are usually five acquisition opportunities associated with ENVISAT's advanced SAR (ASAR) IS2 imaging mode, of which three corresponds to the descending passes. In this mode, in which ASAR is routinely operated, the incidence angle is approximately $23°$. The system has been tested routinely using the 151 track of the ENVISAT's orbit, for which Barcelona is centered in the swath, in a backscattering-like geometry. The data shown in this section correspond to the June 2, 2006 overpass.

Fig. 4 shows the details of the signal received by the direct channel. The upper panel shows the maximum received power for each pulse period during the 7.6-s acquisition window. The azimuth beampattern of the ENVISAT's ASAR system is clearly recovered. The maximum signal arrives 355 ms before the predicted zero-Doppler time, which is within the accuracy expected from the orbital prediction model used and the unknown Doppler centroid. The middle panel shows a 5-ms detail of the signal at the digitizer, showing a train of pulses. The lower panel shows the first 250 samples of two consecutive pulses, in which the chirp waveform is clearly recognizable. Since no explicit PRF signal is available, the pulses are aligned using the nominal pulse-repetition time. Both pulses correspond to the mainlobe, close enough to the zero-Doppler time to guarantee that the interpulse range migration is less than $\lambda/2$. By sampling at $f_s = 33$ MHz, this yields a maximum relative delay of 0.0031 samples. However, the three orders of magnitude larger misalignment observed reveal the lack of synchronism between the data-acquisition system and the transmitter. This error is estimated and corrected while forming the final bistatic raw data.

Fig. 5 shows the first full resolution focused bistatic-SAR image produced by SABRINA next to an aerial photograph of the area. The image shows the intensity of the scattered signal relative to its maximum, and it has been geocoded and projected on a DEM of the area. Topographic contour lines have been overlaid to help the interpretation of the image. The bright region in the image corresponds to the sloped terrain facing the receiver. As expected, regions hidden to the receiver by the
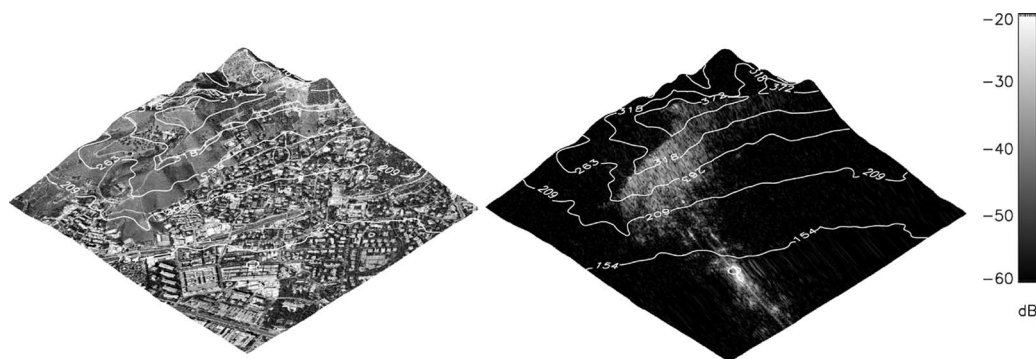
Fig. 5. Aerial picture (left) and bistatic-SAR image (right) of the test area. Both images are georeferenced and projected on the DEM of the area, with topographic contour lines overlaid. The bistatic-SAR image represents the received power referenced to the maximum received power (in decibel scale).
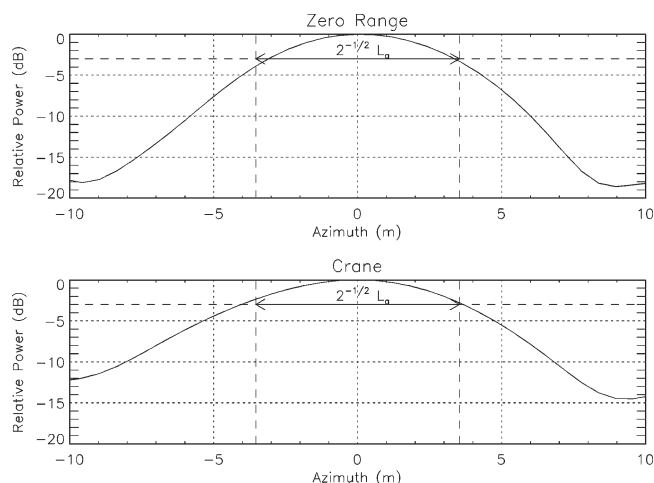

Fig. 6. Detail of azimuth profile of focused image at zero range (top) and of an *ad hoc* point target in the image (bottom).

hills appear dark. There are also several bright spots that can be identified with the positions of a communication tower on top of the Sant Pere Martir Hill and to the construction cranes in the nearby urban area. The maximum of the image is at the position of the receiver and is caused by the sidelobes of the receive antenna and the reflections from nearby objects. The noise floor of the image is roughly 65 dB below the maximum.

The top panel of Fig. 6 shows a detail of the azimuth profile of the relative power at zero range, which is a combination of the leaked direct signal and the reflections of the wall underneath the receive antenna. The bottom panel shows the equivalent profile for an *ad hoc* point target present in the image and corresponding to the position of a construction crane. In both cases, the 3-dB azimuth resolution is very similar to the theoretical resolution given by (6).

V. CONCLUSION AND FUTURE WORK

This letter has presented, at system level, SABRINA: a receiver designed to form a bistatic SAR using ESA's ENVISAT and ERS-2 SAR systems as sensors of opportunity. The emphasis of this letter is on the design challenges derived from the novel bistatic geometry and the lack of explicit synchronization between the receiver and the transmitter. First bistatic images generated by the system, which have been processed using a novel focusing algorithm that combines a subaperture ap-

proach with the classical range-Doppler processing, have been presented. This method uses an approximation of the scene elevation model to precisely focus the bistatic image.

The current system serves as a test bed for the processing algorithms required to focus on the bistatic-SAR images and as a proxy for air- or space-borne bistatic systems. However, its main benefit is to expose the problems associated with the noncooperative bistatic system. Phase-locking, phase-noise characterization, and mitigation and temporal alignment are all problems that require an extensive further study. For example, it is not clear how to correctly separate an oscillator frequency error from an error in the Doppler-centroid estimate. Apart from addressing these issues, future development of SABRINA will be oriented toward interferometric applications.

REFERENCES

[1] I. Walterscheid, J. Ender, A. R. Brenner, and O. Loffeld, "Bistatic SAR processing and experiments," *IEEE Trans. Geosci. Remote Sens.*, vol. 44, no. 10, pp. 2710–2717, Oct. 2006.
[2] O. Loffeld, H. Nies, V. Peters, and S. Knedlik, "Models and useful relations for bistatic SAR processing," *IEEE Trans. Geosci. Remote Sens.*, vol. 42, no. 10, pp. 2031–2038, Oct. 2004.
[3] G. Krieger and M. Younis, "Impact of oscillator noise in bistatic and multistatic SAR," *IEEE Geosci. Remote Sens. Lett.*, vol. 3, no. 3, pp. 424–428, Jul. 2006.
[4] J. Sanz-Marcos, J. Mallorqui, and T. Broquetas, "Bistatic parasitic SAR processor evaluation," in *Proc. Int. Geosci. and Remote Sens. Symp.*, 2004, pp. 3666–3669.
[5] J. Sanz-Marcos, P. Prats, J. Mallorqui, and A. Aguasca, "A subaperture range-Doppler processor for bistatic-fixed-receiver SAR," in *Proc. EUSAR*, 2006. CD-ROM.
[6] J. Curlander and R. N. McDonough, *Synthetic Aperture Radar. Systems and Signal Processing.* Hoboken, NJ: Wiley, 1991, ch. 2.
[7] M. Marti-Neira, M. Caparrini, J. Font-Rossello, S. Lannelongue, and C. Serra-Vallmitjana, "The PARIS concept: An experimental demonstration of sea surface altimetry using GPS reflected signals," *IEEE Trans. Geosci. Remote Sens.*, vol. 39, no. 1, pp. 142–150, Jan. 2001.
[8] F. R. Hoots and R. L. Roehrich, "Models for propagation of NORAD element sets," Aerosp. Defense Center, Peterson AFB, Colorado Springs, CO, Spacetrack Rep. 3, Dec. 1980.
[9] J. Sanz-Marcos, J. Mallorqui, A. Aguasca, and P. Prats, "First ENVISAT and ERS-2 parasitic bistatic fixed receiver SAR images processed with the subaperture range-Doppler algorithm," in *Proc. Int. Geosci. and Remote Sens. Symp.*, 2006, pp. 1840–1843.